Chapter 11: Momentum Advection

11.1 Introduction

If the wind field is specified, as for example in the discussion of Chapter 4, then the advection of a tracer can be considered as a linear problem; it is, at least, linear in the tracer. With *momentum advection*, however, the wind field is both the "advector" and the "advectee." Momentum advection is thus unavoidably nonlinear. Up to now, we have mostly avoided the subject of momentum advection, except for a brief discussion in Chapter 9, which was limited to the one-dimensional case, without rotation. We now consider the advection terms of the momentum equation for the multi-dimensional case, in which vorticity plays a key role. The important new physical ingredient that must be considered in the two-dimensional system is rotation, including both Earth-rotation, f, and the relative vorticity, ζ, associated with the wind field.

The shallow-water equations can be written as

$$\frac{\partial h}{\partial t} + \nabla \cdot \left(h \mathbf{V} \right) = 0 \,, \tag{1}$$

and

$$\frac{\partial \mathbf{V}}{\partial t} + \left(\frac{\zeta + f}{h} \right) \mathbf{k} \times \left(h \mathbf{V} \right) + \nabla \left[K + g \left(h + h_S \right) \right] = 0 \,, \tag{2}$$

where $K \equiv \frac{1}{2} \mathbf{V} \cdot \mathbf{V}$ is the kinetic energy per unit mass,

$$\zeta = \mathbf{k} \cdot \left(\nabla \times \mathbf{V} \right) \tag{3}$$

is the relative vorticity, and

$$f \equiv 2 \Omega \sin \varphi \tag{4}$$

is the Coriolis parameter. In (2), we have multiplied and divided the vorticity term by h, for reasons to be explained later.

The corresponding equations for the zonal and meridional wind components are

$$\frac{\partial u}{\partial t} - \left(\frac{\zeta + f}{h} \right)(hv) + \frac{\partial}{\partial x}\left[K + g\left(h + h_S \right) \right] = 0 \,, \tag{5}$$

and

$$\frac{\partial v}{\partial t} + \left(\frac{\zeta + f}{h} \right)(hu) + \frac{\partial}{\partial y}\left[K + g\left(h + h_S \right) \right] = 0 \,, \tag{6}$$

respectively. Here

$$\mathbf{V} = u\mathbf{i} + v\mathbf{j} \,, \tag{7}$$

where $\mathbf{i}$ and $\mathbf{j}$ are the unit vectors in the zonal and meridional directions, respectively.

When we take the dot product of (2) with $h\mathbf{V}$, the vorticity term contributes nothing *because of the vector identity*

$$(h\mathbf{V}) \cdot \left[\mathbf{k} \times (h\mathbf{V}) \right] = 0 \,, \tag{8}$$

and so we obtain very directly the advective form of the kinetic energy equation, i.e.,

$$h\frac{\partial K}{\partial t} + (h\mathbf{V}) \cdot \nabla\left[K + g\left(h + h_S \right) \right] = 0 \,. \tag{9}$$

By use of the continuity equation (1), we can rewrite (9) in flux form:

$$\frac{\partial}{\partial t}(hK) + \nabla \cdot (h\mathbf{V}K) + (h\mathbf{V}) \cdot \nabla\left[g\left(h + h_S \right) \right] = 0 \,. \tag{10}$$

Similarly, the flux form of the potential energy equation is

$$\frac{\partial}{\partial t}\left[h\left(gh_S + \frac{1}{2}h \right) \right] + \nabla \cdot \left[(h\mathbf{V})\, g\left(h + h_S \right) \right] - (h\mathbf{V}) \cdot \nabla\left[g\left(h + h_S \right) \right] = 0 \,. \tag{11}$$

By adding (10) and (11), we obtain conservation of total energy.

By taking the curl of (2) we can obtain the vorticity equation

$$\frac{\partial \zeta}{\partial t} + \mathbf{V} \cdot \nabla (\zeta + f) + (\zeta + f) \nabla \cdot \mathbf{V} = 0 \,. \tag{12}$$

To derive (12), we have used

$$\mathbf{k} \cdot \nabla \times \left\{ \nabla \left[K + g(h + h_S) \right] \right\} = 0 \,, \tag{13}$$

which is based on another *vector identity*, i.e., the curl of any gradient is zero. Eq. (12) can be rearranged to

$$\frac{\partial (\zeta + f)}{\partial t} + \nabla \cdot \left[\mathbf{V} (\zeta + f) \right] = 0 \,. \tag{14}$$

The combination $\left(\frac{\zeta + f}{h} \right)$ is the potential vorticity for the shallow-water system. As you know, conservation of potential vorticity is a key to the dynamics of balanced flows. The flux form of the potential vorticity equation for shallow water can be obtained simply by rewriting (14) as

$$\frac{\partial}{\partial t} \left[h \left(\frac{\zeta + f}{h} \right) \right] + \nabla \cdot \left[h \mathbf{V} \left(\frac{\zeta + f}{h} \right) \right] = 0 \,. \tag{15}$$

11.2 Aliasing error

We now move to what may appear to be a completely different subject.

Suppose that we have a wave given by the continuous solid line in Fig. 11.1 There are discrete, evenly spaced grid points along the *x*-axis, as shown by the black dots in the figure. The wave has been drawn with a wave length of $(4/3)\Delta x$, corresponding to a wave number of $\frac{3\pi}{2\Delta x}$. Because $(4/3)\Delta x < 2\Delta x$, the wave is too short to be represented on the grid. What the grid points "see" instead is not the wave represented by the solid line, but rather the wave of wavelength $4\Delta x$, as indicated by the dashed line (again drawn as a continuous function of *x*). At the grid points, the wave of length $4\Delta x$ takes exactly the values that the wave of $(4/3)\Delta x$ would take at those same grid points, if it could be represented on the grid at all. This misrepresentation of a wavelength too short to be represented on the grid is called "aliasing error." *Aliasing is a high wave number (or frequency) masquerading as a low wave number (or frequency).* In the example of Fig. 11.1, aliasing occurs because the grid is too coarse to resolve the wave of length $(4/3)\Delta x$. Another way of saying this is that the wave is not adequately "sampled" by the grid. *Aliasing error is always due to inadequate sampling.*

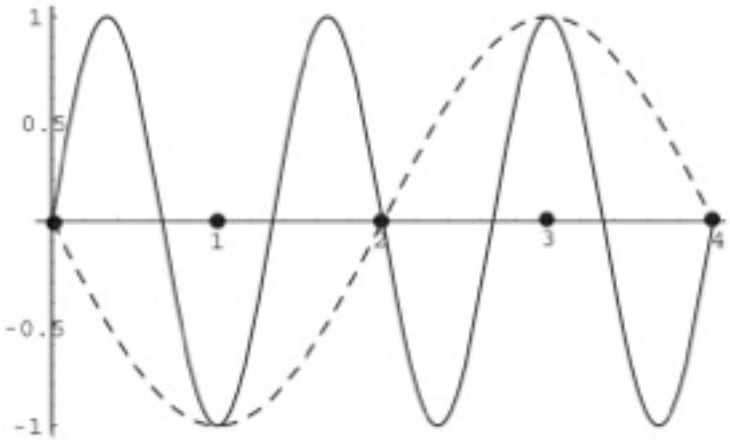

Figure 11.1: An example of aliasing error. Distance along the horizontal axis is measured in units of Δx . The wave given by the solid line has a wave length of $(4/3)\Delta x$. This is shorter than $2\Delta x$, and so the wave cannot be represented on the grid. Instead, the grid "sees" a wave of wavelength $4\Delta x$, as indicated by the dashed line. Note that the $4\Delta x$ -wave is "upside-down."

Aliasing error can be important in observational studies, because observations taken "too far apart" in space (or time) can make a short wave (or high frequency) appear to be a longer wave (or lower frequency). Fig. 11.2 is an example, from real life. The blue curve in the figure makes it appear that the precipitation rate averaged over the global tropics fluctuates with a period of 23 days and an amplitude approaching 1mm day^{-1} . If this tropical precipitation oscillation (TPO) were real, it would be one of the most amazing phenomena in atmospheric science, and its discoverer would be on the cover of *Rolling Stone*. But alas, the TPO is bogus, even though you can see it with your own eyes in Fig. 11.2, and even though the figure is based on real data. The satellite from which the data was collected has an orbit that takes it over the same point on Earth *at the same time of day* once every 23 days. Large regions of the global tropics have a strong diurnal (i.e., day-night) oscillation of the precipitation rate. This high-frequency diurnal signal is aliased onto a much lower frequency, i.e., 23 days, because *the sampling by the satellite is inadequate* to resolve the diurnal cycle.

Aliasing error is also important in modeling, when we try to solve either non-linear equations or linear equations with variable coefficients. The reason is that the product terms (or other nonlinear terms) in such equations can produce, or "try to produce," waves shorter than the grid can represent. For example, suppose that we have two modes on a one-dimensional grid, given by

$$A\left(x_j\right) = \hat{A}e^{ikj\Delta x} \text{ and } B\left(x_j\right) = \hat{B}e^{ilj\Delta x}, \tag{16}$$

respectively. Here the wave numbers of A and B are denoted by k and l, respectively. We assume that k and l both "fit" on the grid in question. If we combine A and B linearly, e.g., form

$$\alpha A + \beta B \,, \tag{17}$$

where α and β are spatially constant coefficients, then no "new" waves are generated; k and l continue to be the only wave numbers present. In contrast, if we multiply A and B together, then we generate the new wave number, $k + l$:

$$AB = \hat{A}\hat{B}e^{i(k+l)j\Delta x} \,, \tag{18}$$

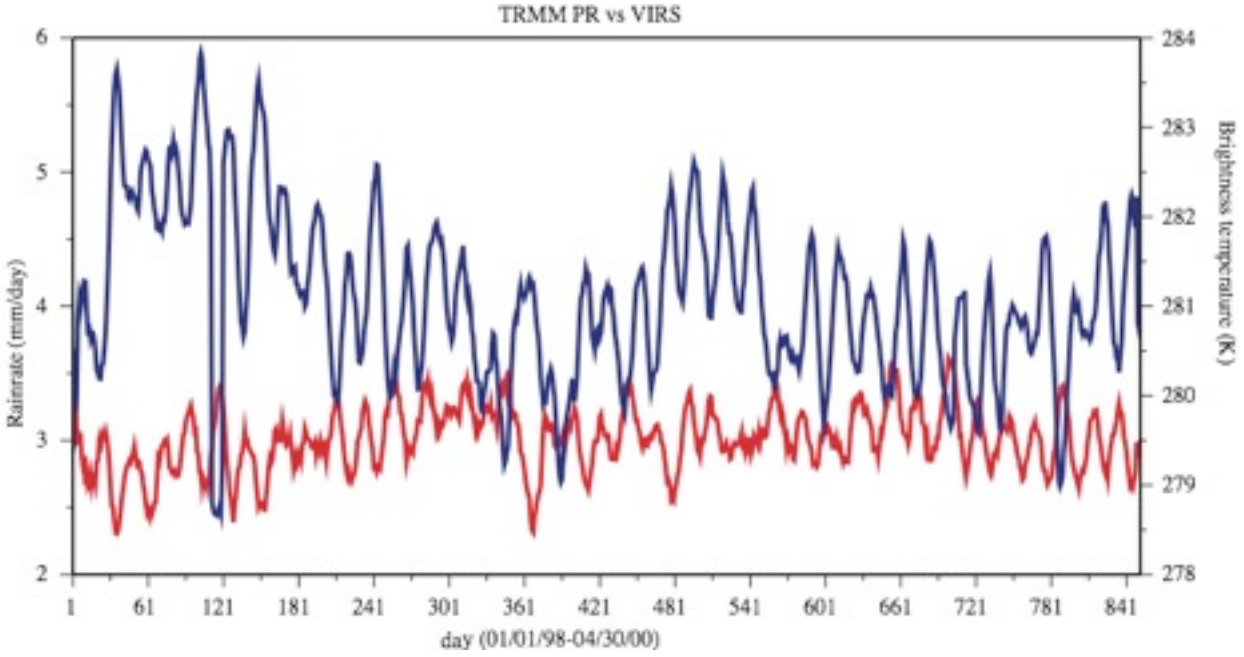

Figure 11.2: An example of aliasing in the analysis of observations. The blue curve shows the precipitation rate, averaged over the global tropics (20° S to 20° N), and the red curve shows a the thermal radiation in the 11.8 μm band, averaged over the same region. The horizontal axis is time, and the period covered is slightly more than two years. The data were obtained from the TRMM (Tropical Rain Mapping Mission) satellite. The obvious oscillation in both curves, with a period close to 23 days, is an artifact due to aliasing. See the text for further explanation.

Other nonlinear operations such as division, exponentiation, etc., will also generate new wave numbers. It can easily happen that $(k+l)\Delta x > \pi$, in which case the new mode created by multiplying A and B together does not fit on the grid. *What actually happens in such a case is that the new mode is aliased onto a mode that* ***does*** *fit on the grid.*

Because the shortest wavelength that the grid can represent is $L = 2\Delta x$, the maximum representable wave number is $k_{\max} \equiv \pi / \Delta x$. What happens when a wave with $k > k_{\max}$ is produced, e.g., through nonlinear interactions? Since $2k_{\max}\Delta x = 2\pi$, we can assume that

$2k_{\max} > k > k_{\max}$. (A wave with $k > 2k_{\max} = 2\pi$ "folds back.") We can write the expression $\sin(kj\Delta x)$ as

$$\begin{aligned}\sin\left[k(j\Delta x)\right] &= \sin\left[\left(2k_{\max} - 2k_{\max} + k\right)j\Delta x\right] \\ &= \sin\left[2\pi j - \left(2k_{\max} - k\right)j\Delta x\right] \\ &= \sin\left[-\left(2k_{\max} - k\right)j\Delta x\right] \\ &= \sin\left[k^*(j\Delta x)\right],\end{aligned} \tag{19}$$

where $k^* \equiv -\left(2k_{\max} - k\right)$. Note that $0 < k^* < k_{\max}$ because, by assumption, $2k_{\max} > k > k_{\max}$. Similarly,

$$\cos\left[k(j\Delta x)\right] = \cos\left[k^*(j\Delta x)\right]. \tag{20}$$

Eqs. (18) - (19) show that the wave of wave number $k > k_{\max}$ is interpreted (or misinterpreted) by the grid as a wave of wave number k^*. The minus sign means that the phase change per Δx is

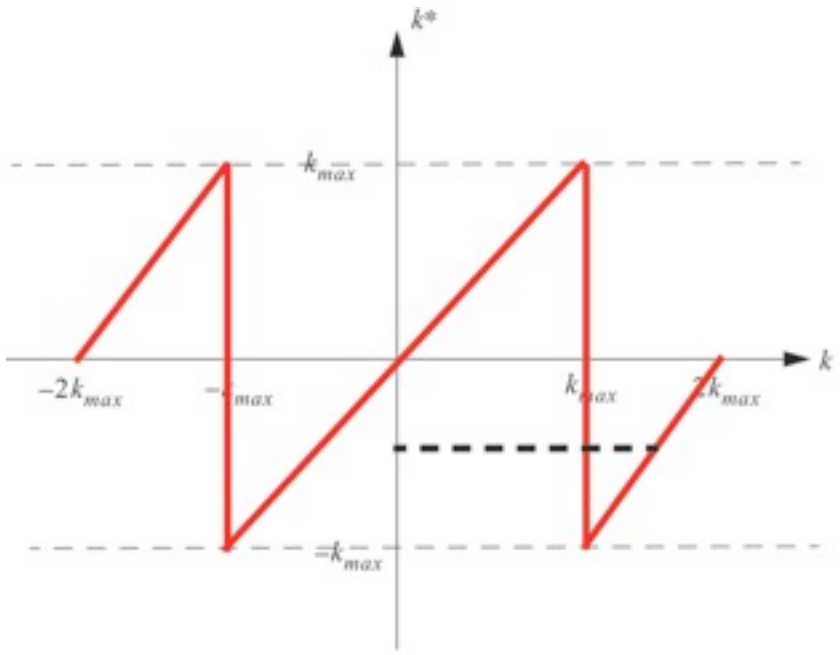

Figure 11.3: The red line is a plot of k^* on the vertical axis, versus k on the horizontal axis. The dashed black line connects $k = \frac{3\pi}{2\Delta x}$ with $k^* = \frac{\pi}{2\Delta x}$, corresponding to the example of Fig. 11.1.

reversed, or "backwards." Fig. 11.3 illustrates how k^* varies with k. For $-k_{\max} \le k \le k_{\max}$, we

simply have $k^* = k$. For $k > k_{\max}$, we get $0 > k^* > -k_{\max}$, and so on.

In the example of Fig. 11.1, $L = (4/3)\Delta x$ so $k = 2\pi / L$. Therefore $k^* \equiv -(2k_{\max} - k) = \frac{2\pi}{\Delta x} - \frac{3\pi}{2\Delta x} = \frac{\pi}{2\Delta x}$, which means that $L^* = 4\Delta x$, as we have already surmised by inspection of Fig. 11.1.

For $k < k_{\max}$, the phase change, as j increases by one, is less than π. This is shown in Fig. 11.4 a. For $k > k_{\max}$, the phase change as j increases by one is greater than π. This is shown in Fig. 11.4 b. For $k > k_{\max}$, the dot in the figure appears to move clockwise, i.e., "backwards." This is a manifestation of aliasing that is familiar from the movies. It also explains why the minus sign appears in Eq. (19).

Aliasing error is important in part because it is the root cause of what is often called "nonlinear computational instability." This instability occurs with nonlinear equations, but as explained below it can also occur with linear equations that have spatially variable coefficients. A better name for the instability would be "aliasing instability." An example is presented in the

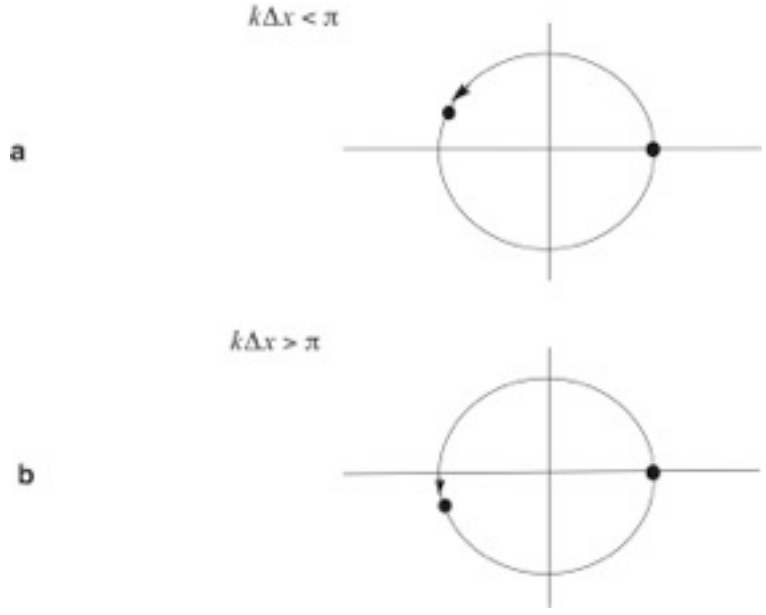

Figure 11.4: The phase change per grid point for: a) $k\Delta x < \pi$, and b) $k\Delta x > \pi$.

next section.

11.3 Advection by a variable, non-divergent current

What does aliasing have to do with vorticity and kinetic energy? The connections will be made in this and the following sections.

Suppose that an arbitrary variable q is advected in two dimensions on a plane, so that

$$\frac{\partial q}{\partial t} + \mathbf{V} \cdot \nabla q = 0 \,, \tag{21}$$

where the flow is assumed to be non-divergent, i.e.,

$$\nabla \cdot \mathbf{V} = 0 \,. \tag{22}$$

Two-dimensional non-divergent flow is a not-too-drastic idealization of the large-scale circulation of the atmosphere. In view of (22), we can describe $\mathbf{V}$ in terms of a stream function ψ, such that

$$\mathbf{V} = \mathbf{k} \times \nabla \psi \tag{23}$$

Substituting (23) into (21), we get

$$\frac{\partial q}{\partial t} + \left(\mathbf{k} \times \nabla \psi \right) \cdot \nabla q = 0 \,. \tag{24}$$

Using the vector identity

$$\left(\mathbf{V}_1 \times \mathbf{V}_2 \right) \cdot \mathbf{V}_3 = \mathbf{V}_2 \cdot \left(\mathbf{V}_3 \times \mathbf{V}_1 \right) , \tag{25}$$

which holds for any three vectors, we set $\mathbf{V}_1 \equiv \mathbf{k}$, $\mathbf{V}_2 \equiv \nabla \psi$, and $\mathbf{V}_3 \equiv \nabla q$, to obtain

$$\left(\mathbf{k} \times \nabla \psi \right) \cdot \nabla q = \mathbf{k} \cdot \left(\nabla \psi \times \nabla q \right) . \tag{26}$$

With the use of (26), we can re-write (21) as

$$\frac{\partial q}{\partial t} + J\left(\psi, q \right) = 0 \,, \tag{27}$$

or alternatively as

$$\frac{\partial q}{\partial t} = J\left(q, \psi \right) . \tag{28}$$

Here J is the *Jacobian* operator, which is defined by

$$J(A,B) \equiv \mathbf{k} \cdot (\nabla A \times \nabla B) \tag{29}$$

$$= -\mathbf{k} \cdot \nabla \times (A \nabla B) \tag{30}$$

$$= \mathbf{k} \cdot \nabla \times (B \nabla A), \tag{31}$$

for arbitrary A and B. Note that

$$J(A,B) = -J(B,A), \tag{32}$$

which can be deduced from (31), and this has been used to go from (27) to (28). From the definition of the Jacobian, it follows that $J(p,q) = 0$ if either A or B is constant.

In Cartesian coordinates, we can write $J(A,B)$, in the following three alternative forms, which are suggested by the forms of (31):

$$J(A,B) = \frac{\partial A}{\partial x}\frac{\partial B}{\partial y} - \frac{\partial A}{\partial y}\frac{\partial B}{\partial x} \tag{33}$$

$$= \frac{\partial}{\partial y}\left(B\frac{\partial A}{\partial x}\right) - \frac{\partial}{\partial x}\left(B\frac{\partial A}{\partial y}\right) \tag{34}$$

$$= \frac{\partial}{\partial x}\left(A\frac{\partial B}{\partial y}\right) - \frac{\partial}{\partial y}\left(A\frac{\partial B}{\partial x}\right). \tag{35}$$

These will be used later.

Let an overbar denote an average over a two-dimensional domain that has no boundaries (e.g., a sphere or a torus), or on the boundary of which either A or B is constant. You should be able to prove the following:

$$\overline{J(A,B)} = 0, \tag{36}$$

$$\overline{AJ(A,B)} = 0, \tag{37}$$

$$\overline{BJ(A,B)} = 0. \tag{38}$$

Multiplying both sides of the advection equation (28) by q, we obtain

$$\frac{1}{2}\frac{\partial q^2}{\partial t} = qJ(q,\psi) = J\left(\frac{1}{2}q^2,\psi\right). \tag{39}$$

Integrating over the entire area, we see that

$$\int J\left(\frac{1}{2}q^2,\psi\right)ds = -\int \mathbf{V}\cdot\nabla\frac{1}{2}q^2\,ds = -\int \nabla\cdot\left(\mathbf{V}\frac{1}{2}q^2\right)ds = 0\,, \tag{40}$$

if the domain is surrounded by a rigid boundary where the normal component of $\mathbf{V}$ is zero, or if the domain is periodic.

When ψ is a prescribed spatially varying function, (28) is linear, although with variable coefficients. As already mentioned, what is often called "non-linear" instability is actually a type of instability that can occur in the numerical integration of a linear equation with variable coefficients, as well as in the numerical integration of nonlinear equations. What this instability really amounts to is a spurious growth of waves due in part to the aliasing error arising from the multiplication of the finite difference analogs of *any* two spatially varying quantities.

To illustrate the problem, we begin by writing down a differential-difference version of (28), on a plane, using a simple finite-difference approximation for the Jacobian. For simplicity, we take $\Delta x = \Delta y = d$. We investigate the particular choice

$$\frac{dq_{i,j}}{dt} = \left[J_1(q,\psi)\right]_{i,j} \tag{41}$$

where

$$\left[J_1(q,\psi)\right]_{i,j} \equiv \frac{1}{4d^2}\left[\left(q_{i+1,j}-q_{i-1,j}\right)\left(\psi_{i,j+1}-\psi_{i,j-1}\right)-\left(q_{i,j+1}-q_{i,j-1}\right)\left(\psi_{i+1,j}-\psi_{i-1,j}\right)\right]. \tag{42}$$

You should confirm for yourself that (42) is a finite-difference approximation to (28). Later we are going to discuss several other finite-difference approximations for the Jacobian. The particular finite-difference Jacobian given in (42) is based on (33), and is called J_1. It will come up again in the later discussion.

Now we work through a simple example of aliasing instability, which was invented by Phillips (1959; also see Lilly, 1965). We combine (41) and (42) to obtain

$$\frac{dq_{i,j}}{dt} \equiv \frac{1}{4d^2}\Big[\big(q_{i+1,j}-q_{i-1,j}\big)\big(\psi_{i,j+1}-\psi_{i,j-1}\big)-\big(q_{i,j+1}-q_{i,j-1}\big)\big(\psi_{i+1,j}-\psi_{i-1,j}\big)\Big] \tag{43}$$

Assume that the solution, $q_{i,j}(t)$, is of the form

$$q_{i,j}(t)=\left[C(t)\cos\frac{\pi i}{2}+S(t)\sin\frac{\pi i}{2}\right]\sin\frac{2\pi j}{3}. \tag{44}$$

The use of such assumption may appear strange; it will be justified later. For all t, let $\psi_{i,j}$ be *prescribed* as

$$\psi_{i,j}=U\cos(\pi i)\sin\left(\frac{2\pi j}{3}\right). \tag{45}$$

In (45), we are prescribing a time-independent but *spatially variable* advecting current. We have often prescribed the advecting current in earlier chapters, but until now it has always been spatially uniform. Because $\psi_{i,j}$ is prescribed, the model that we are considering here is linear, but it has spatially variable coefficients. The forms of $q_{i,j}$ and $\psi_{i,j}$ given by (44) and (45) are

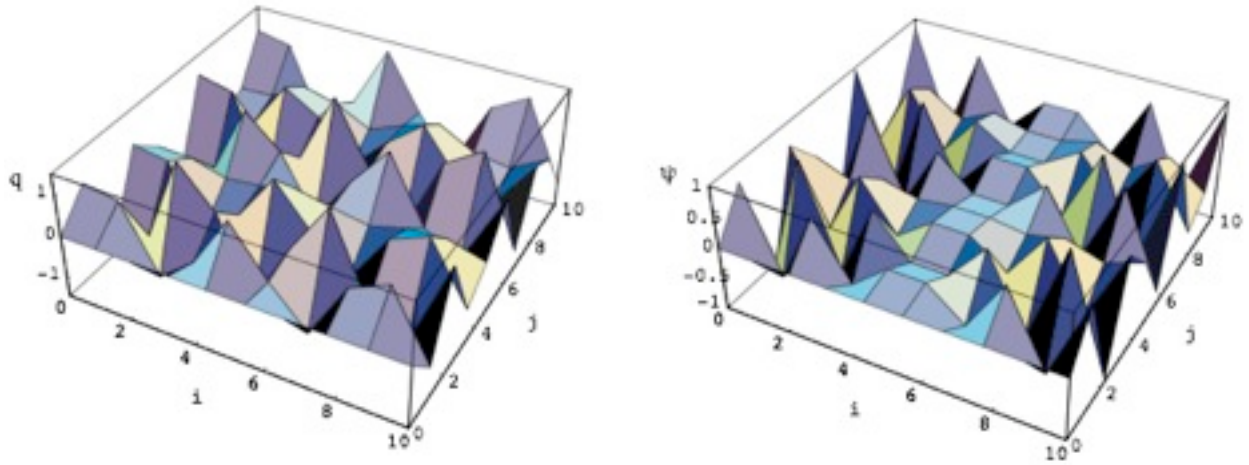

Figure 11.5: Plots of the functions $q_{i,j}(t=0)$ and $\psi_{i,j}$ given by (11.43) and (11.44), respectively. For plotting purposes, we have used $C=S=U=1$. The functions have been evaluated only for integer values of i and j, which gives them a jagged appearance. Nevertheless it is fair to say that they are rather ugly. This is the sort of thing that can appear in your simulations as a result of aliasing instability.

plotted in Fig. 11.5. They are nasty functions.

Because (45) specifies $\psi_{i,j}$ to have a wavelength of $2d$ in the x-direction, we can simplify (43) to

$$\frac{\partial q_{i,j}}{\partial t} = \frac{1}{4d^2}\left(q_{i+1,j} - q_{i-1,j}\right)\left(\psi_{i,j+1} - \psi_{i,j-1}\right). \tag{46}$$

From (44), we see that

$$q_{i+1,j} - q_{i-1,j} = \left\{C\left[\cos\frac{\pi(i+1)}{2} - \cos\frac{\pi(i-1)}{2}\right] + S\left[\sin\frac{\pi(i+1)}{2} - \sin\frac{\pi(i-1)}{2}\right]\right\}\sin\frac{2\pi j}{3}$$

$$= 2\left(-C\sin\frac{\pi i}{2} + S\cos\frac{\pi i}{2}\right)\sin\frac{2\pi j}{3}. \tag{47}$$

Here we have used some trigonometric identities. Similarly, we can show that

$$\psi_{i,j+1} - \psi_{i,j-1} = U\cos(\pi i)\,2\cos\left(\frac{2\pi j}{3}\right)\sin\left(\frac{2\pi}{3}\right)$$

$$= \sqrt{3}U\cos(\pi i)\cos\left(\frac{2\pi j}{3}\right). \tag{48}$$

As already mentioned, (48) holds for all t.

The product of (47) and (48) gives the right-hand side of (46), which can be written, using trigonometric identities, as

$$\frac{dq_{i,j}}{dt} = \frac{\sqrt{3}}{4d^2}U\left\{-C\left[\sin\left(\frac{3\pi i}{2}\right) - \sin\left(\frac{\pi i}{2}\right)\right] + S\left[\cos\left(\frac{3\pi i}{2}\right) + \cos\left(\frac{\pi i}{2}\right)\right]\right\}\sin\left(\frac{4\pi j}{3}\right)$$

$$= \frac{\sqrt{3}}{4d^2}U\left[C\sin\left(\frac{\pi i}{2}\right) + S\cos\left(\frac{\pi i}{2}\right)\right]\sin\left(\frac{4\pi j}{3}\right). \tag{49}$$

Now we make the important observation that the wave number in the y-direction, denoted by l, satisfies

$$\frac{4\pi j}{3} = ly = l(jd). \tag{50}$$

Therefore,

$$ld = \frac{4\pi}{3} > \pi \ .$$

(51)

This shows that the product on the right-hand side of (46) has produced a wave number in the y-direction that is too short to be represented on the grid. In other words, aliasing occurs. According to our earlier analysis, this wave will be interpreted by the grid as having wave number $-\left(2l_{\max} - l\right) = -\left(2\pi / 3d\right)$. Therefore (49) can be re-written as

$$\frac{dq_{i,j}}{dt} = -\frac{\sqrt{3}U}{4d^2}\left(C\sin\frac{\pi i}{2} + S\cos\frac{\pi i}{2}\right)\sin\frac{2\pi j}{3} \ .$$

(52)

Rewriting (49) as (52) is a key step in our analysis, because this is where aliasing enters. In doing the problem algebraically, we have to put in the aliasing "by hand."

According to (52) the spatial form of $\frac{dq_{i,j}}{dt}$ agrees with the assumed form of $q_{i,j}$, given by (44). This means that the spatial shape of $q_{i,j}$ does not change with time, *thus justifying our assumption (44).* In order to recognize that the spatial shape of $q_{i,j}$ does not change with time, we had to take into account that aliasing occurs.

If we now simply differentiate (44) with respect to time, and substitute the result into the left-hand side of (52), we get

$$\frac{dC}{dt}\cos\frac{\pi i}{2}\sin\frac{2\pi j}{3} + \frac{dS}{dt}\sin\frac{\pi i}{2}\sin\frac{2\pi j}{3} = -\frac{\sqrt{3}}{4d^2}U\left(C\sin\frac{\pi i}{2} + S\cos\pi\frac{i}{2}\right)\sin\frac{2\pi j}{3} \ .$$

(53)

Note that time derivatives of *C* and *S* appear on the left-hand side of (53). Using the linear independence of the sine and cosine functions, we see from (53) that

$$\frac{dC}{dt} = -\frac{\sqrt{3}}{4d^2}US, \text{ and } \frac{dS}{dt} = -\frac{\sqrt{3}}{4d^2}UC \ .$$

(54)

From (54), it follows that

$$\frac{d^2C}{dt^2} = \sigma^2 C \text{ and } \frac{d^2S}{dt^2} = \sigma^2 S \ ,$$

(55)

where $\sigma \equiv \frac{\sqrt{3}U}{4d^2}$. According to (55), C and S will grow exponentially. This demonstrates that the finite-difference scheme is unstable. The unstable modes will have the form given by (44) and plotted in Fig. 11.5.

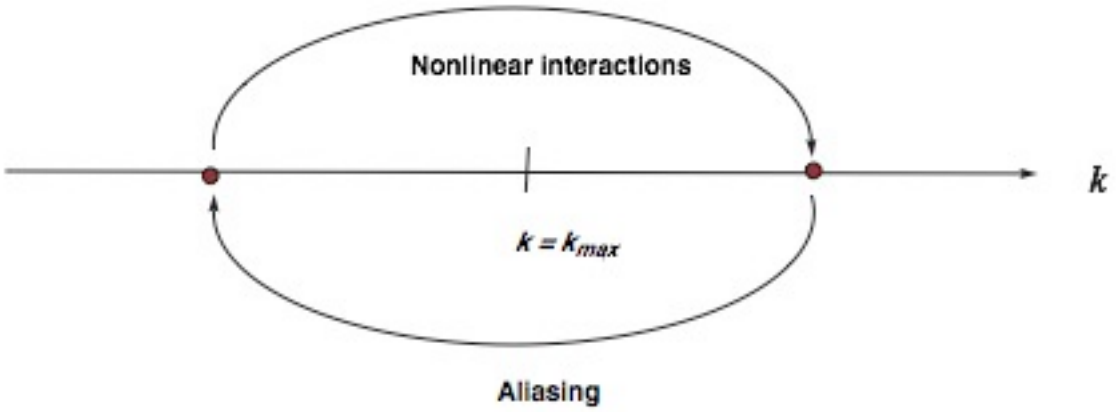

Figure 11.6: Sketch illustrating the mechanism of aliasing instability.

Fig. 11.6 summarizes the mechanism of this aliasing instability. Nonlinear interactions feed energy into waves that cannot be represented on the grid. Aliasing causes this energy to "fold back" onto scales that do fit on the grid, but typically these are rather small scales that are not well resolved and suffer from large truncation errors. In the example given, the truncation errors lead to further production of energy on scales too small to be represented, etc.

Note, however, that *if the numerical scheme conserved energy, the total amount of energy could not increase, and the instability would be prevented, even though aliasing would still occur, and even though the truncation errors for the smallest scales would still be large.* In the example discussed above, we used J_1. Later we demonstrate that J_1 does not conserve energy. As we will discuss, some other finite-difference Jacobians do conserve energy. Instability would not occur with those Jacobians.

Further general insight into this type of instability can be obtained by investigating the truncation error of the expression on the right side of (42). This can be expressed as

$$\left(\frac{dq}{dt}\right)_{i,j} = \left[J_1(q,\psi)\right]_{i,j}$$
$$= \left[J(q,\psi)\right]_{i,j} + \frac{d^2}{6}\left[\frac{\partial q}{\partial x}\frac{\partial^3 \psi}{\partial y^3} - \frac{\partial q}{\partial y}\frac{\partial^3 \psi}{\partial x^3} + \frac{\partial^3 q}{\partial x^3}\frac{\partial \psi}{\partial y} - \frac{\partial^3 q}{\partial y^3}\frac{\partial \psi}{\partial x}\right]_{i,j} + O\left(d^4\right). \tag{56}$$

The second line is obtained by Taylor series expansion. Note the second-order accuracy. Multiplying (56) by q, integrating over the whole domain, and making use of (39), (40) and

(50), we find, after repeated integration by parts and a page or so of algebra, that when we use J_1, the second-order part of the truncation error causes the square of q to increase at the rate

$$\frac{1}{2}\frac{d}{dt}\int q^2 ds = \frac{d^2}{4}\int \frac{\partial^2 \psi}{\partial x \partial y}\left[\left(\frac{\partial q}{\partial x}\right)^2 - \left(\frac{\partial q}{\partial y}\right)^2\right] ds + \int O\left(d^4\right) ds \,. \tag{57}$$

This means that, for $\frac{\partial^2 \psi}{\partial x \partial y} > 0$, q^2 will falsely grow with time if $\left(\frac{\partial q}{\partial x}\right)^2$ is bigger than $\left(\frac{\partial q}{\partial y}\right)^2$, in an overall sense. In such a situation, instability will occur. The scheme will blow up *locally,* in the particular portions of the domain where $\frac{\partial^2 \psi}{\partial x \partial y} > 0$.

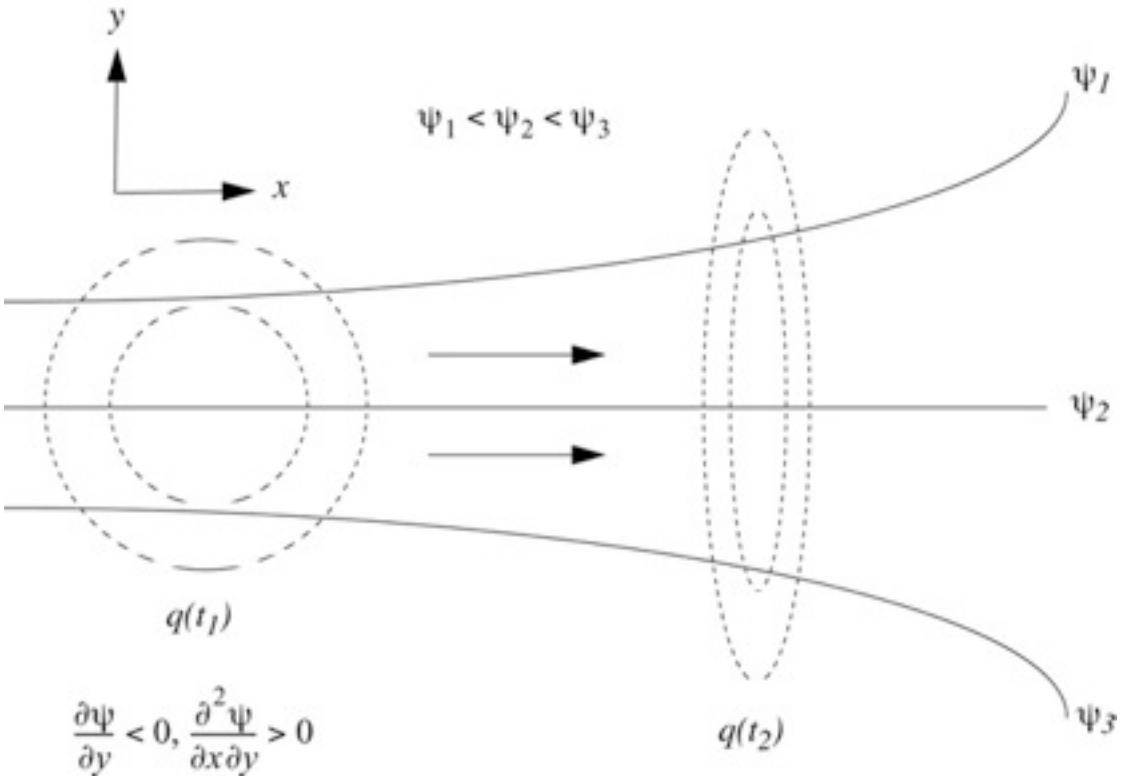

Figure 11.7: Schematic illustration of the mechanism of aliasing instability. Nonlinear interactions feed energy into scales too small to be represented on the grid, and this energy folds back through aliasing into scales that can be represented. The process feeds on itself. This can cause the total amount of energy to increase, unless the scheme is energy conserving.

Now look at Fig. 11.7. In the figure, the streamlines are given such that $\psi_1 < \psi_2 < \psi_3$, so that $\left(\partial \psi / \partial y\right) < 0$, and. This resembles the "exit" region of the jet stream. [Note: The stream function sketched in Fig. 11.7 does not correspond to (45).] In fact, the solution of the

differential-difference equation tends to prefer a positive value of the integrand of the right-hand side of (57), as illustrated schematically in Fig. 11.7. Notice that at t_2, $\frac{\partial q}{\partial x}$ becomes greater than it was at t_1, and the reverse is true for $\frac{\partial q}{\partial y}$. Therefore, although at t_1 the expression $\int \frac{\partial^2 \psi}{\partial x \partial y}\left[\left(\frac{\partial q}{\partial x}\right)^2 - \left(\frac{\partial q}{\partial y}\right)^2\right] ds$ vanishes, at t_2 it has become positive. From (58), it can be seen that the area-integrated q^2 tends to increase with time, whereas it is invariant in the differential case.

In contrast to the linear computational instabilities discussed earlier in this course, *aliasing instability has nothing to do with time truncation error*. Making the time step shorter cannot prevent the instability, which can occur, in fact, even in the time-continuous case. The example we have just considered illustrates this fact, because we have left the time derivatives in continuous form.

A number of methods have been proposed to prevent or control aliasing instability. One approach is to prevent aliasing. As will be discussed in Chapter 13, aliasing error can actually be eliminated in a spectral model, at least for terms that involve only "quadratic" aliasing, i.e., aliasing that arises from the multiplication of two spatially varying fields; this will be discussed later. Aliasing instability can also be prevented without eliminating aliasing, however.

Phillips (1959) suggested that aliasing instability can be prevented if a Fourier analysis of the predicted fields is made after each time step, and all waves of wave number $k > k_{\max}/2$ are simply discarded. With this "filtering" method, Phillips could guarantee absolutely no aliasing error due to quadratic nonlinearities, because the shortest possible wave would have wave number $k_{\max}/2$ (his maximum wave number) and thus any wave generated by quadratic nonlinearities would have a wave number of at most $k_{\max}$. This method is strongly dissipative, however, because the filter removes variance.

Others have suggested that use of a dissipative scheme, such as the Lax-Wendroff scheme, can overcome aliasing instability. Experience shows that this is not true. The damping of a dissipative scheme depends on the value of $\frac{c\Delta t}{\Delta x}$, but aliasing instability can occur even for $\frac{c\Delta t}{\Delta x} \to 0$.

A third approach is to use a sign-preserving advection scheme, as discussed in Chapter 4, and advocated by Smolarkeiwicz (1991).

A fourth approach is to use space-differencing schemes for the advection terms that are designed to conserve the square of the advected quantity. The "energy approach" to checking stability, discussed in Chapter 2, ensures that such schemes are computationally stable. This

approach has the advantage that stability is ensured simply by mimicking a property of the exact equations.

To prevent aliasing instability with the momentum equations, we can use finite-difference schemes that conserve either kinetic energy, or enstrophy (squared vorticity), or both. This approach was developed by Arakawa (1966). It will be explained below, after a digression in which we discuss the nature of two-dimensional nondivergent flows.

11.4 Fjortoft's Theorem

When the flow is nondivergent, so that (22) is satisfied, the vorticity equation, (23), reduces to

$$\frac{\partial}{\partial t}(\zeta + f) = -\mathbf{V} \cdot \nabla(\zeta + f) \,. \tag{58}$$

This says that the absolute vorticity is simply advected by the mean flow. We also see that only the sum $(\zeta + f)$ matters for the vorticity equation; henceforth we just replace $(\zeta + f)$ by ζ, for simplicity. Using Eq. (23), we can show that the vorticity and the stream function are related by

$$\zeta \equiv \mathbf{k} \cdot (\nabla \times \mathbf{V}) = \nabla^2 \psi \,. \tag{59}$$

This relationship was used as an example of a boundary-value problem, back in Chapter 6. Eq. (5) can be rewritten as

$$\frac{\partial \zeta}{\partial t} = -\nabla \cdot (\mathbf{V}\zeta) \,, \tag{60}$$

or, alternatively, as

$$\frac{\partial \zeta}{\partial t} = J(\zeta, \psi) \,. \tag{61}$$

From (60) we see that the domain-averaged vorticity is conserved:

$$\frac{d\overline{\zeta}}{dt} = \overline{\frac{\partial \zeta}{\partial t}} = 0 \,. \tag{62}$$

By combining (61) and (38), we obtain

$$\overline{\zeta \frac{\partial \zeta}{\partial t}} = 0 \,, \tag{63}$$

from which it follows that the domain-average of the enstrophy is also conserved:

$$\frac{d}{dt}\left(\frac{1}{2}\overline{\zeta^2}\right)=0\,.$$

(64)

Similarly, from (61) and (37) we find that

$$\overline{\psi\frac{\partial\zeta}{\partial t}}=0\,.$$

(65)

To see what this implies, substitute (59) into (65), to obtain

$$\overline{\psi\frac{\partial}{\partial t}\nabla^2\psi}=0\,.$$

(66)

This is equivalent to

$$\begin{aligned}0&=\overline{\psi\frac{\partial}{\partial t}\nabla^2\psi}\\&=\overline{\psi\frac{\partial}{\partial t}\left[\nabla\cdot(\nabla\psi)\right]}\\&=\overline{\psi\nabla\cdot\frac{\partial}{\partial t}\nabla\psi}\\&=\overline{\nabla\cdot\left(\psi\frac{\partial}{\partial t}\nabla\psi\right)}-\overline{\nabla\psi\cdot\frac{\partial}{\partial t}\nabla\psi}\\&=-\overline{\frac{\partial}{\partial t}\left(\frac{1}{2}|\nabla\psi|^2\right)}.\end{aligned}$$

(67)

Eq. (68) is a statement of kinetic energy conservation, showing that (66) implies kinetic energy conservation. In fact, it can be shown that, for a purely rotational flow,

$$\bar{K}=\overline{\psi\zeta}\,.$$

(68)

Since both kinetic energy and enstrophy are conserved in frictionless two-dimensional flows, their ratio is also conserved, and has the dimensions of a length squared:

$$\frac{\text{energy}}{\text{enstrophy}}\sim\frac{L^2t^{-2}}{t^{-2}}=L^2\,.$$

(69)

This length can be interpreted as the typical scale of energy-containing vortices, and (69) states that it is invariant. The implication is that energy does not cascade in frictionless two-dimensional flows; it "stays where it is" in wave number space.

The exchanges of energy and enstrophy among different scales in two-dimensional turbulence were studied by Ragnar Fjortoft (1953), a Norwegian meteorologist who obtained some very fundamental and famous results, which can be summarized in a simplified way as

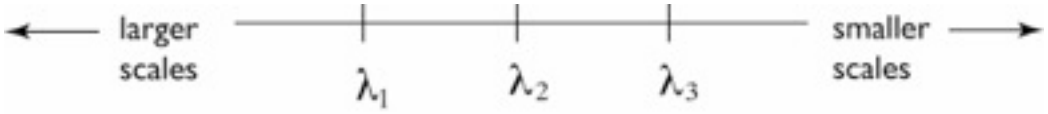

Figure 11.8: Diagram used in the explanation of Fjortoft's (1953) analysis of the exchanges of energy and enstrophy among differing scales in two-dimensional motion.

follows. Consider three equally spaced wave numbers, as shown in Fig. 11.8. By "equally spaced," we mean that

$$\lambda_2 - \lambda_1 = \lambda_3 - \lambda_2 = \Delta\lambda \,. \tag{70}$$

The enstrophy, E, is

$$E = E_1 + E_2 + E_3 \,, \tag{71}$$

and the kinetic energy is

$$K = K_1 + K_2 + K_3 \,. \tag{72}$$

It can be shown that

$$E_n = \lambda^2{}_n K_n \,, \tag{73}$$

where λ_n is a wave number, and the subscript n denotes a particular Fourier component. Suppose that kinetic energy is redistributed, i.e.,

$$K_n \to K_n + \delta K_n \,, \tag{74}$$

such that

$$\sum \delta K_n = 0 \,, \tag{75}$$

$$\sum \delta E_n = 0 \,,$$

(76)

and note from (73) that

$$\delta E_n = \lambda^2{}_n \delta K_n \,.$$

(77)

It follows that

$$\delta K_1 + \delta K_3 = -\delta K_2 \,,$$

(78)

$$\begin{aligned} \lambda_1^2 \delta K_1 + \lambda_3^2 \delta K_3 &= -\lambda_2^2 \delta K_2 \\ &= \lambda_2^2 \left(\delta K_1 + \delta K_3 \right) . \end{aligned}$$

(79)

Collecting terms, we find that

$$\frac{\delta K_3}{\delta K_1} = \frac{\lambda^2{}_2 - \lambda^2{}_1}{\lambda^2{}_3 - \lambda^2{}_2} \,.$$

(80)

Using (70), we get

$$\frac{\delta K_3}{\delta K_1} = \frac{\lambda_2 + \lambda_1}{\lambda_3 + \lambda_2} < 1 \,.$$

(81)

Eq. (81) shows that the energy transferred to higher wave numbers $\left(\delta K_3 \right)$ is less than the energy transferred to lower wave numbers $\left(\delta K_1 \right)$. This conclusion rests on both (75) and (76), i.e., on both energy conservation and enstrophy conservation. The implication is that kinetic energy actually "migrates" from higher wave numbers to lower wave numbers, i.e., from smaller scales to larger scales.

We now perform a similar analysis for the enstrophy. As a first step, we use (77) and (81) to write

$$\begin{aligned} \frac{\delta E_3}{\delta E_1} &= \frac{\lambda_3^2}{\lambda_1^2} \left(\frac{\lambda_2 + \lambda_1}{\lambda_3 + \lambda_2} \right) \\ &= \frac{\left(\lambda_2 + \Delta\lambda \right)^2}{\left(\lambda_2 - \Delta\lambda \right)^2} \frac{\left(\lambda_2 - \frac{1}{2} \Delta\lambda \right)}{\left(\lambda_2 + \frac{1}{2} \Delta\lambda \right)} > 1 \,. \end{aligned}$$

(82)

To show that this ratio is greater than one, we demonstrate that $\frac{\delta E_3}{\delta E_1} = a \cdot b \cdot c$, where a, b, and c are each greater than one. We can choose:

$$a = \frac{\lambda_2 + \Delta\lambda}{\lambda_2 - \Delta\lambda} > 1, \tag{83}$$

$$b = \frac{\lambda_2 - \frac{1}{2}\Delta\lambda}{\lambda_2 - \Delta\lambda} > 1, \tag{84}$$

$$c = \frac{\lambda_2 + \Delta\lambda}{\lambda_2 + \frac{1}{2}\Delta\lambda} > 1. \tag{85}$$

The conclusion is that enstrophy cascades to higher wave numbers in two-dimensional turbulence. Of course, such a cascade ultimately leads to enstrophy dissipation by viscosity.

When viscosity acts on two-dimensional turbulence, enstrophy is dissipated but kinetic energy is (almost) not. Then the denominator of (69) decreases with time, while the numerator remains nearly constant. It follows that the length scale, *L*, will tend to increase with time. This means that the most energetic vortices will become larger. This is an "anti-cascade" of kinetic energy. The implication is that two-dimensional turbulence tends to remain smooth, so that the kinetic energy of the atmosphere tends to remain on large, quasi-two-dimensional scales, instead of cascading down to small scales where it can be dissipated.

In three-dimensions, vorticity is not conserved because of stretching and twisting, and enstrophy is not conserved because of stretching (although it is unaffected by twisting). Vortex stretching causes small scales to gain energy at the expense of larger scales. As a result, kinetic energy cascades in three-dimensional turbulence. Ultimately the energy is converted from kinetic to internal by the viscous force. This is relevant to small-scale atmospheric circulations, such as boundary-layer eddies and cumulus cells.

In summary, vorticity and enstrophy are conserved in two-dimensional flow but not in three-dimensional flow. Kinetic energy is conserved under inertial processes in both two-dimensional and three-dimensional flows. Because two-dimensional flows are obliged to conserve both energy and enstrophy, they "have fewer options" than do three-dimensional flows. In particular, a kinetic energy cascade cannot happen in two dimensions. What happens instead is an enstrophy cascade. Enstrophy is dissipated but kinetic energy is (almost) not.

Because kinetic energy does not cascade in two-dimensional flow, the motion remains smooth and is dominated by "large" eddies. This is true with the continuous equations, and we want it to be true in our models as well.

11.5 Kinetic energy and enstrophy conservation in two-dimensional non-divergent flow

Lorenz (1960) suggested that energy-conserving finite-difference schemes would be advantageous in efforts to produce realistic numerical simulations of the general circulation of the atmosphere. Arakawa (1966) developed a method for numerical simulation of two-dimensional, purely rotational motion, that conserves both kinetic energy and enstrophy. His method has been very widely used. The following is a summary of Arakawa's approach.

We begin by writing down a spatially discrete version of (61), keeping the time derivative in continuous form:

$$\begin{aligned}\sigma_{\boldsymbol{i}} \frac{d\zeta_{\boldsymbol{i}}}{dt} &= \sigma_{\boldsymbol{i}} J_{\boldsymbol{i}}(\zeta,\psi) \\ &= \sum_{\boldsymbol{i}'}\sum_{\boldsymbol{i}''} c_{\boldsymbol{i},\boldsymbol{i}',\boldsymbol{i}''}\zeta_{\boldsymbol{i}+\boldsymbol{i}'}\psi_{\boldsymbol{i}+\boldsymbol{i}''} \ .\end{aligned} \tag{86}$$

Here the area of grid cell $\boldsymbol{i}$ is denoted by $\sigma_{\boldsymbol{i}}$. The $c_{\boldsymbol{i},\boldsymbol{i}',\boldsymbol{i}''}$ are "coefficients" (we will refer to them that way) that must be specified to define the finite-difference scheme, following the approach that we first introduced in Chapter 2. The bold subscripts are two-dimensional counters that can be used to specify a grid cell on a two-dimensional grid by giving a single number, again as discussed in Chapter 2. For later reference, with double subscripts, (86) would become

$$\sigma_{i,j}\frac{d\zeta_{i,j}}{dt} = \sum_{j'}\sum_{i'}\sum_{j''}\sum_{i''}\left(c_{i,j;i+i',j+j';i+i'',j+j''}\right)\zeta_{i+i',j+j'}\psi_{i+i'',j+j''} \ . \tag{87}$$

The second line of (86) looks a little mysterious and requires some explanation. As can be seen by inspection of (33), the Jacobian operator, $J(\zeta,\psi)$, involves derivatives of the vorticity, multiplied by derivatives of the stream function. We can anticipate, therefore, that the form we choose for the finite-difference Jacobian at the point $\boldsymbol{i}$ will involve products of the vorticity at some nearby grid points with the stream function at other nearby grid points. We have already seen an example of this in (42). Such products appear in (86). The neighboring grid points can be specified in (86) by assigning appropriate values to $\boldsymbol{i}'$ and $\boldsymbol{i}''$. As you can see from the subscripts, $\boldsymbol{i}'$ picks up vorticity points, and $\boldsymbol{i}''$ picks up stream function points. The $c_{\boldsymbol{i},\boldsymbol{i}',\boldsymbol{i}''}$ are "interaction coefficients." Their form will be chosen later. It is by appropriate choices of the $c_{\boldsymbol{i},\boldsymbol{i}',\boldsymbol{i}''}$ that we can construct an approximation to the Jacobian. The double sum in (86) essentially picks out the combinations of ζ and ψ, at neighboring grid points, that we wish to bring into our finite-difference operator. This is similar to the notation that we used in Chapter 2, but a bit more complicated.

Of course, there is nothing about the form of (86) that shows that it is actually a consistent finite-difference approximation to the Jacobian operator; all we can say at this point is that (86) has the *potential* to be a consistent finite-difference approximation to the Jacobian, if

we choose the interaction coefficients properly. The coefficients can be chosen to give any desired order of accuracy (in the Taylor series sense), using the methods discussed in Chapter 2.

The form of (86) is sufficiently general that it is impossible to tell what kind of grid is being used. It could be a rectangular grid on a plane, or a latitude-longitude grid on the sphere, or something more exotic like a geodesic grid on the sphere (to be discussed in Chapter 12).

As an example, consider the finite-difference Jacobian J_1 , introduced in Eq. (42). Applying J_1 to vorticity advection on a square grid with grid spacing d , we can write, corresponding to (86),

$$d^2 \frac{d\zeta_{i,j}}{dt} = d^2 \left\{ \frac{1}{4d^2} \left[\left(q_{i+1,j} - q_{i-1,j} \right) \left(\psi_{i,j+1} - \psi_{i,j-1} \right) - \left(q_{i,j+1} - q_{i,j-1} \right) \left(\psi_{i+1,j} - \psi_{i-1,j} \right) \right] \right\}$$

$$= \frac{1}{4} \left(q_{i+1,j}\psi_{i,j+1} - q_{i+1,j}\psi_{i,j-1} - q_{i-1,j}\psi_{i,j+1} + q_{i-1,j}\psi_{i,j-1} - q_{i,j+1}\psi_{i+1,j} + q_{i,j+1}\psi_{i-1,j} + q_{i,j-1}\psi_{i+1,j} - q_{i,j-1}\psi_{i-1,j} \right).$$

By inspection of the second line above, and comparing with (86), we see that for J_1 each value of $c_{i,j;i+i',j+j';i+i'',j+j''}$ is either $1/4$ or $-1/4$. The values are as follows:

$$\begin{aligned}
c_{i,j;i+1,j;i,j+1} &= +\frac{1}{4}, \\
c_{i,j;i+1,j;i,j-1} &= -\frac{1}{4}, \\
c_{i,j;i-1,j;i,j+1} &= -\frac{1}{4}, \\
c_{i,j;i-1,j;i,j-1} &= +\frac{1}{4}, \\
c_{i,j;i,j+1;i+1,j} &= -\frac{1}{4}, \\
c_{i,j;i,j+1;i-1,j} &= +\frac{1}{4}, \\
c_{i,j;i,j-1;i+1,j} &= +\frac{1}{4}, \\
c_{i,j;i,j-1;i-1,j} &= -\frac{1}{4}.
\end{aligned} \tag{88}$$

Look carefully at the subscripts. As an example, you should be able to see that $c_{i,j;i+1,j;i,j+1}$ specifies the contribution of the vorticity east of the point (i,j) combined with the stream function north of the point (i,j) to the time rate of change of the vorticity at the point (i,j).

With the uniform square grid on a plane, the coefficients are very simple, as seen in (88). The same methods can be applied to very different cases, however, such as nonuniform grids on a sphere. Any finite-difference Jacobian should give zero if both of the input fields are spatially constant, so from (87), we require that

$$0 = \sum_{i'} \sum_{i''} c_{i,i',i''} \quad \text{for all } \boldsymbol{i}, \tag{89}$$

i.e., the sum of the coefficients is zero for all $\boldsymbol{i}$. The requirement (88) would emerge automatically if we enforced, for example, second-order accuracy of the Jacobian. You can confirm that J_1 satisfies (89).

Similarly, in case the vorticity field is spatially constant, it should remain so for all time. From (86), this requirement takes the form

$$0 = \sum_{i'} \sum_{i''} c_{i,i',i''} \psi_{i+i''} \text{ for all } \boldsymbol{i}. \tag{90}$$

Eq. (90) can be interpreted as the condition that the motion is nondivergent. *Note that (90) must be true regardless of how the stream function varies in space.* This is only possible if each grid-point value of $\psi_{i+i''}$ appears more than once (at least twice) in the sum. Then we can arrange that the "total coefficient" multiplying $\psi_{i+i''}$, i.e., the sum of the two or more $c_{i,i',i''}$'s that multiply $\psi_{i+i''}$, is zero. In that case, the actual values of $\psi_{i+i''}$ have no effect on the sum in (90). You can confirm that J_1 satisfies (90).

In order to ensure conservation of the domain-averaged vorticity under advection, we must require that

$$0 = \sum_{i} \sum_{i'} \sum_{i''} c_{i,i',i''} \zeta_{i+i'} \psi_{i+i''}. \tag{91}$$

Here we have a triple sum, because we are taking a spatial average. Eq. (91) is thus different in kind from (89) and (90). Eq. (91) is required to be true *regardless of how the vorticity and stream function vary in space.* This is only possible if each product $\zeta_{i+i''}\psi_{i+i''}$ appears more than once in the sum, such that the sum of the two or more $c_{i,i',i''}$ s that multiply each $\zeta_{i+i''}\psi_{i+i''}$, is zero. In that case, the actual values of $\zeta_{i+i''}\psi_{i+i''}$ have no effect on the sum in (91).

With a little work, we can show that J_1 satisfies (91). Each term of the triple sum in (91) involves the product of the vorticity and a stream function. Each product will appear exactly twice when we form the sum. In order for (91) to be satisfied for arbitrary distributions of the vorticity and the stream function, we need the two contributions from each product to cancel in

the sum, i.e., their coefficients must be equal and opposite. As pointed out above, $c_{i,j;i+1,j;i,j+1}$ specifies the contributions of the vorticity at $i+1, j$ and the stream function at $i, j+1$ to the time rate of change of the vorticity at the point i, j . Similarly, $c_{i+1,j+1;i+1,j;i,j+1}$ specifies the contributions of the vorticity at $i+1, j$ and the stream function at $i, j+1$ to the time rate of

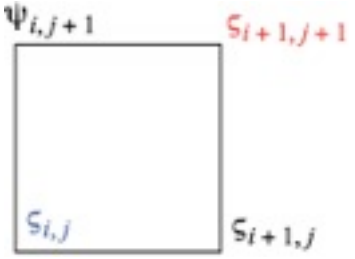

Figure 11.9: Stencil used in the discussion of vorticity conservation for J_1 . See text for details.

change of the vorticity at the point $i+1, j+1$. See Fig. 11.9. Cancellation will occur if the coefficients satisfy

$$c_{i,j;i+1,j;i,j+1} = -c_{i+1,j+1;i+1,j;i,j+1} . \tag{92}$$

To see whether or not this is the case, we use the essential fact that *the scheme is the same for all points on the grid*. We can "shift" the stencil for the scheme from one grid cell to another by adding any integer to all i subscripts for each coefficient, and adding a (generally different) integer to all j subscripts, without changing the numerical values of the coefficients. For example, the value of $c_{i+1,j+1;i+1,j;i,j+1}$ remains unchanged if we subtract one from each i subscript and one from each j subscript. In other words,

$$c_{i+1,j+1;i+1,j;i,j+1} = c_{i,j;i,j-1;i-1,j} . \tag{93}$$

Therefore, the requirement (92) is equivalent to

$$c_{i,j;i+1,j;i,j+1} = -c_{i,j;i,j-1;i-1,j} . \tag{94}$$

What has been accomplished by subtracting one from each subscript is that in the result, i.e., (94), *both of the coefficients are associated with the time-rate of change of the vorticity at the point* (i, j), and so both of them are explicitly listed in (88). The meaning of (94) is that the "up, right" coefficient is equal to minus the "down-left" coefficient. By symmetry, we can anticipate that the "up-left" coefficient will also be equal to minus the "down-right" coefficient. Inspection of (88) shows that (94) is indeed satisfied. Similar results apply for the remaining terms. In this way, we can satisfy ourselves that J_1 conserves vorticity.

Returning to the general problem, what we are going to do now is find a way to enforce finite-difference analogs of (64) and (66):

$$\begin{aligned} 0 &= \sum_i \sigma_i \zeta_i J_i(\zeta,\psi) \\ &= \sum_i \zeta_i \left(\sum_{i'} \sum_{i''} c_{i,i',i''} \zeta_{i+i'} \psi_{i+i''} \right) \\ &= \sum_i \left(\sum_{i'} \sum_{i''} c_{i,i',i''} \zeta_i \zeta_{i+i'} \psi_{i+i''} \right), \end{aligned} \tag{95}$$

$$\begin{aligned} 0 &= \sum_i \sigma_i \psi_i J_i(\zeta,\psi) \\ &= \sum_i \psi_i \left(\sum_{i'} \sum_{i''} c_{i,i',i''} \zeta_{i+i'} \psi_{i+i''} \right) \\ &= \sum_i \left(\sum_{i'} \sum_{i''} c_{i,i',i''} \zeta_{i+i'} \psi_i \psi_{i+i''} \right). \end{aligned} \tag{96}$$

By enforcing these two requirements, we can ensure conservation of enstrophy and kinetic energy in the finite-difference model. The requirements can be met, as we will see, by suitable choices of the interaction coefficients. Eqs. (95) and (96) look daunting, though, because they involve triple sums. How in the world are we ever going to work this out?

Inspection of (95) shows that the individual terms of the triple sum are going to involve products of vorticities at pairs of grid points. With this in mind, we go back to (87) and rewrite the scheme as

$$\begin{aligned} \sigma_i J_i(\zeta,\psi) &= \sum_{i'} \sum_{i''} c_{i,i',i''} \zeta_{i+i'} \psi_{i+i''} \\ &= \sum_{i'} a_{i,i+i'} \zeta_{i+i'} , \end{aligned} \tag{97}$$

where, by definition,

$$a_{i,i+i'} \equiv \sum_{i''} c_{i,i',i''} \psi_{i+i''} . \tag{98}$$

Using (98), we can write (97) times ζ_i as

$$\sigma_i \zeta_i J_i(\zeta,\psi) = \sum_{i'} a_{i,i+i'} \zeta_i \zeta_{i+i'} . \tag{99}$$

Here we have simply taken ζ_i inside the sum, which we can do because the sum is over i', not i. From this point it is straightforward to enforce (95), which can be rewritten as

$$0 = \sum_i \left(\sum_{i'} a_{i,i+i'} \zeta_i \zeta_{i+i'} \right). \tag{100}$$

Think of the outer sum in (100) as a "DO" loop. As we sweep over the grid, each product $\zeta_i \zeta_{i+i''}$ will enter the sum exactly twice. We can specify the vorticities any way we want, e.g., when we set up the initial conditions, so the only way to make sure that (100) is satisfied regardless of the spatial distribution of the vorticity is to force these two contributions to the sum to be equal and opposite, i.e., we must take

$$a_{i,i+i'} = -a_{i+i',i} \text{ for all } i \text{ and } i'. \tag{101}$$

By enforcing (101), we can ensure enstrophy conservation. Notice that Eq. (101) implies that

$$a_{i,i} = 0 \text{ for all } i. \tag{102}$$

With the definition (98), we can rewrite the nondivergence condition (90) as

$$0 = \sum_{i'} a_{i,i+i'} \text{ for all } i. \tag{103}$$

A scheme that satisfies (101) and (102) will also satisfy (103), which means that the nondivergence condition will be satisfied "automatically."

Kinetic energy conservation can be guaranteed by a very similar approach. We rewrite (87) as

$$\begin{aligned} \sigma_i J_i(\zeta, \psi) &= \sum_{i'} \sum_{i''} c_{i,i',i''} \zeta_{i+i'} \psi_{i+i''} \\ &= \sum_{i''} b_{i,i+i''} \psi_{i+i''}, \end{aligned} \tag{104}$$

where

$$b_{i,i+i''} \equiv \sum_{i'} c_{i,i',i''} \zeta_{i+i'}. \tag{105}$$

The requirement for kinetic energy conservation, (96), can then be written as

$$0 = \sum_i \left(\sum_{i''} b_{i,i+i''} \psi_i \psi_{i+i''} \right),$$

(106)

which is analogous to (100). By an argument similar to that given above, we find that

$$b_{i,i+i''} = -b_{i+i'',i} \text{ all } i \text{ and } i'' .$$

(107)

is necessary to ensure kinetic energy conservation.

Actually, that's not quite true. To ensure kinetic energy conservation, we must also make sure that the finite-difference analog of (67) holds, i.e.,

$$\sum_i \left(\sigma_i \psi_i \frac{d\zeta_i}{dt} \right) = -\sum_i \left[\sigma_i \frac{d}{dt} \left(\frac{1}{2} |\nabla \psi|_i^2 \right) \right],$$

(108)

so that we can mimic with the finite-difference equations the derivation that we did with the continuous equations. In order to pursue this objective, we have to define a finite-difference Laplacian.

As an example, we use the simplest possibility, assuming a square grid with grid spacing d:

$$\begin{aligned} \zeta_{i,j} &= \left(\nabla^2 \psi \right)_{i,j} \\ &\equiv \frac{1}{d^2} \left(\psi_{i+1,j} + \psi_{i-1,j} + \psi_{i,j+1} + \psi_{i,j-1} - 4\psi_{i,j} \right). \end{aligned}$$

(109)

Here we have reverted to a conventional double-subscripting scheme, for clarity. We also define a finite-difference kinetic energy by

$$\begin{aligned} K_{i,j} &\equiv \frac{1}{2} |\nabla \psi|_{i,j}^2 \\ &\equiv \frac{1}{4d^2} \left[\left(\psi_{i+1,j} - \psi_{i,j} \right)^2 + \left(\psi_{i,j+1} - \psi_{i,j} \right)^2 + \left(\psi_{i,j} - \psi_{i-1,j} \right)^2 + \left(\psi_{i,j} - \psi_{i,j-1} \right)^2 \right] \end{aligned}$$

(110)

Because the right-hand side of (110) is a sum of squares, we are guaranteed that kinetic energy is non-negative. By substitution of (109) and (110) into (108), and after a little algebra, we can demonstrate that (108) is actually satisfied.

The results obtained above are very general; they apply on an arbitrary grid, and on a two-dimensional domain of arbitrary shape. It could be a sphere.

This is all fine, as far as it goes, but we still have some very basic and important business to attend to: We have not yet ensured that the sum in (87) is actually a consistent finite-difference approximation to the Jacobian operator. The approach that we will follow is to write down three independent finite-difference Jacobians and then identify, by inspection, the *c*'s in (87). When we say that the Jacobians are "independent," we mean that it is not possible to write any one of the three as a linear combination of the other two. The three finite-difference Jacobians are:

$$\left(J_1\right)_{i,j} = \frac{1}{4d^2}\Big[\left(\zeta_{i+1,j} - \zeta_{i-1,j}\right)\left(\psi_{i,j+1} - \psi_{i,j-1}\right) - \left(\zeta_{i,j+1} - \zeta_{i,j-1}\right)\left(\psi_{i+1,j} - \psi_{i-1,j}\right)\Big], \tag{111}$$

$$\begin{aligned}\left(J_2\right)_{i,j} = \frac{1}{4d^2}\Big[&-\left(\zeta_{i+1,j+1} - \zeta_{i+1,j-1}\right)\psi_{i+1,j} + \left(\zeta_{i-1,j+1} - \zeta_{i-1,j-1}\right)\psi_{i-1,j} \\ &+\left(\zeta_{i+1,j+1} - \zeta_{i-1,j+1}\right)\psi_{i,j+1} - \left(\zeta_{i+1,j-1} - \zeta_{i-1,j-1}\right)\psi_{i,j-1}\Big],\end{aligned} \tag{112}$$

$$\begin{aligned}\left(J_3\right)_{i,j} = \frac{1}{4d^2}\Big[&\zeta_{i+1,j}\left(\psi_{i+1,j+1} - \psi_{i+1,j-1}\right) - \zeta_{i-1,j}\left(\psi_{i-1,j+1} - \psi_{i-1,j-1}\right) \\ &-\zeta_{i,j+1}\left(\psi_{i+1,j+1} - \psi_{i-1,j+1}\right) + \zeta_{i,j-1}\left(\psi_{i+1,j-1} - \psi_{i-1,j-1}\right)\Big].\end{aligned} \tag{113}$$

These can be interpreted as finite-difference analogs to the right-hand sides of (33) - (35), respectively. We can show that all three of these finite-difference Jacobians vanish if either of the input fields is spatially constant, and all three conserve vorticity, i.e., they all satisfy (91).

What we need to do next is identify the coefficients *a* and *b* for each of (110), (111), and (112), and then check to see whether the requirements (101) and (106) are satisfied by any of them. In order to understand more clearly what these requirements actually mean, look at Fig.

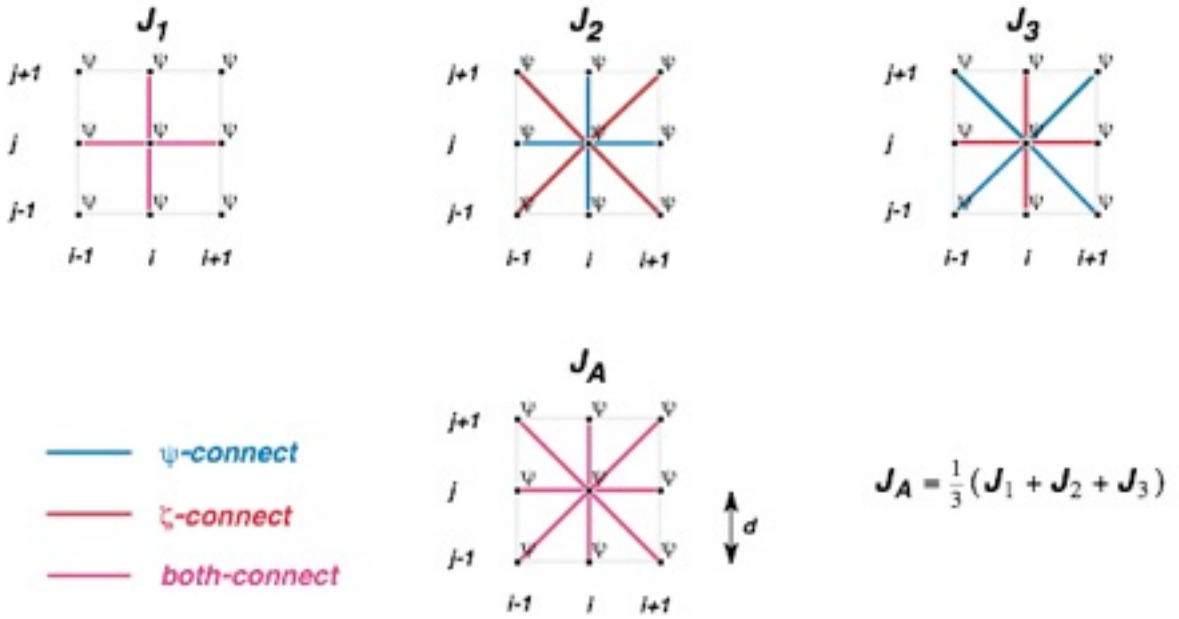

Figure 11.10: The central point in each figure is (i,j). Stream function and vorticity are both defined at each of the mesh points indicated by the black dots. The colored lines represent contributions to $J_{i,j}$ from ψ, ζ, or both, from the various neighboring points.

11.11. The Jacobians J_1, J_2, and J_3 are represented in the top row of the figure. The colored lines show how each Jacobian at the point (i,j) is influenced (or not) by the stream function and vorticity at the various neighboring points. We begin by rewriting (97) using the conventional double-subscript notation and equating it to $(J_1)_i$

$$\begin{aligned}\sigma_{i,j}(J_1)_{i,j}(\zeta,\psi) &= \sum_{i'}\sum_{j'}\sum_{i''}\sum_{j''} c_{i',j';i'',j''}\zeta_{i,j;i+i',j+j'}\psi_{i+i'',j+j''} \\ &= \sum_{i'}\sum_{j'} a_{i,j;i+i',j+j'}\zeta_{i,j;i+i',j+j'} \\ &= \frac{1}{4}\left[\left(\zeta_{i+1,j}-\zeta_{i-1,j}\right)\left(\psi_{i,j+1}-\psi_{i,j-1}\right)-\left(\zeta_{i,j+1}-\zeta_{i,j-1}\right)\left(\psi_{i+1,j}-\psi_{i-1,j}\right)\right] \\ &= \frac{1}{4}\Big[\zeta_{i+1,j}\left(\psi_{i,j+1}-\psi_{i,j-1}\right)-\zeta_{i-1,j}\left(\psi_{i,j+1}-\psi_{i,j-1}\right) \\ &\quad -\zeta_{i,j+1}\left(\psi_{i+1,j}-\psi_{i-1,j}\right)+\zeta_{i,j-1}\left(\psi_{i+1,j}-\psi_{i-1,j}\right)\Big].\end{aligned} \tag{114}$$

Here we have used

$$\sigma_{i,j} = d^2 . \tag{115}$$

In the last line of (114), we have collected the coefficients of each distinct value of the vorticity. By inspection of (13) and comparison with (97), we can read off the as for J_1:

$$a_{i,j;i+1,j} = \frac{1}{4}\left(\psi_{i,j+1} - \psi_{i,j-1}\right), \tag{116}$$

$$a_{i,j;i-1,j} = -\frac{1}{4}\left(\psi_{i,j+1} - \psi_{i,j-1}\right), \tag{117}$$

$$a_{i,j;i,j+1} = -\frac{1}{4}\left(\psi_{i+1,j} - \psi_{i-1,j}\right), \tag{118}$$

$$a_{i,j;i,j-1} = \frac{1}{4}\left(\psi_{i+1,j} - \psi_{i-1,j}\right), \tag{119}$$

Are these consistent with (101)? To find out, replace i by $i+1$ in (117); this gives:

$$a_{i+1,j;i,j} = -\frac{1}{4}\left(\psi_{i+1,j+1} - \psi_{i+1,j-1}\right). \tag{120}$$

Now simply compare (119) with (115), to see that (101) is *not* satisfied by J_1. This shows that J_1 does not conserve enstrophy.

We can interpret that $a_{\boldsymbol{i},\boldsymbol{i}+\boldsymbol{i}'}$ denotes ζ-interactions of point $\boldsymbol{i}$ with point $\boldsymbol{i}+\boldsymbol{i}'$, while $a_{i+i',i}$ denotes ζ-interactions of point $\boldsymbol{i}+\boldsymbol{i}'$ with point $\boldsymbol{i}$. When we compare $a_{\boldsymbol{i},\boldsymbol{i}+\boldsymbol{i}'}$ with $a_{\boldsymbol{i}+\boldsymbol{i}',\boldsymbol{i}}$, it is like peering along one of the red lines in Fig. 11.10, first outward from the point $(i.j)$, to one of the other points, and then back toward the point $(i.j)$. The condition (101) on the a s essentially means that all such interactions are "equal and opposite" allowing suitable algebraic cancellations to occur when we sum over all points. The condition (106) on the b s has a similar interpretation.

By proceeding as illustrated above, we can reach the following conclusions:

- J_1 conserves neither enstrophy nor kinetic energy;
- J_2 conserves enstrophy but not kinetic energy; and
- J_3 conserves kinetic energy but not enstrophy.

It looks like we are out of luck.

We can form a new Jacobian, however, by combining J_1, J_2, and J_3 with weights, as follows:

$$J_A = \alpha J_1 + \beta J_2 + \gamma J_3 , \tag{121}$$

such that

$$\alpha + \beta + \gamma = 1 . \tag{122}$$

With three unknown coefficients, and only one constraint, namely (122), we are free to satisfy two additional constraints; and we take these to be (101) and (107). In this way, we can show that J_A will conserve both enstrophy and kinetic energy if we choose

$$\alpha = \beta = \gamma = 1/3 . \tag{123}$$

The composite Jacobian, J_A, is often called the "Arakawa Jacobian."

Fig. 11.11 shows the results of tests with J_1, J_2, and J_3, and also with three other Jacobians called J_4, J_5, and J_6, as well as with J_A. The leapfrog time-differencing scheme was used in these tests; the influence of time differencing on the conservation properties of the schemes will be discussed later; it is minor, as long as we do not violate the criteria for linear computational instability. The various space-differencing schemes do indeed display the conservation properties expected on the basis of the preceding analysis.

The approach outlined above yields a conservative second-order accurate (in space) finite-difference approximation to the Jacobian. Arakawa (1966) also showed how to obtain the corresponding conservative Jacobian with fourth-order accuracy.

The preceding analysis shows how vorticity, kinetic energy and enstrophy can be conserved under advection in numerical simulations of two-dimensional non-divergent flow. In practice, however, we have to consider the presence of divergence. When the flow is divergent, vorticity and enstrophy are not conserved, but potential vorticity and potential enstrophy are conserved.

In Chapter 4, we concluded that, by suitable choice of the interpolated "cell-wall" values of an arbitrary advected quantity, A, it is possible to conserve exactly one non-trivial function of A, i.e., $F(A)$, in addition to A itself. Conserving more than A and one $F(A)$ was not possible

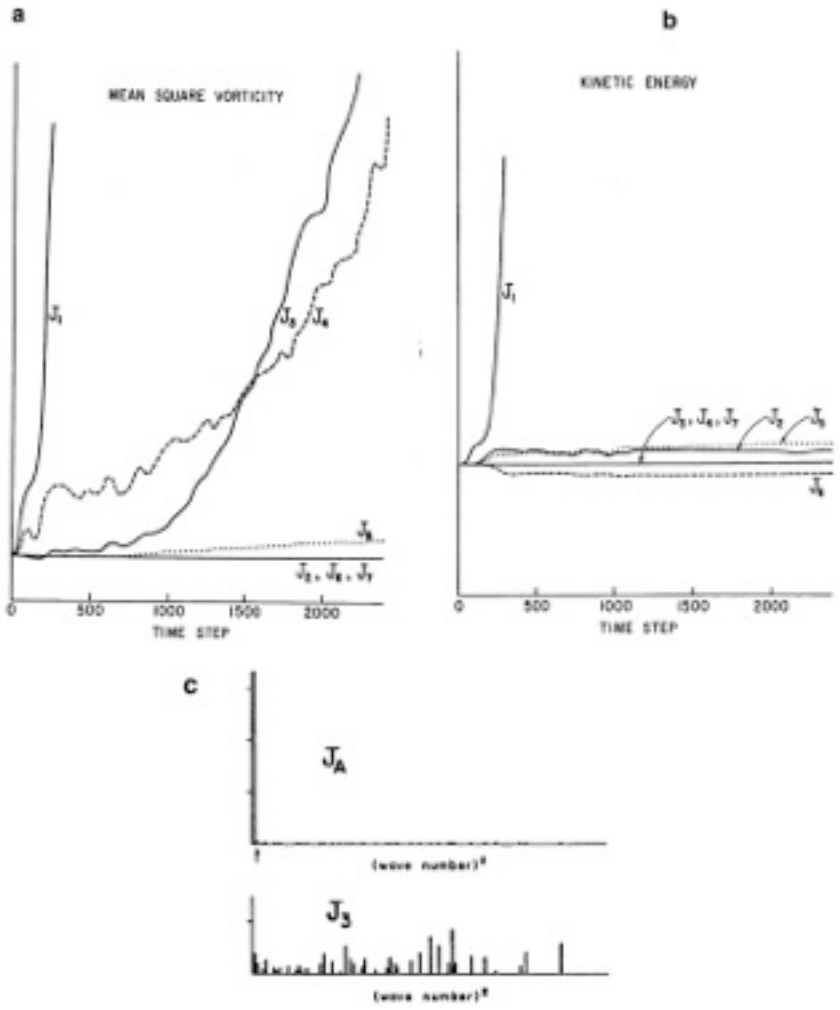

Figure 11.11: Results of tests with the various finite-difference Jacobians. Panel c shows that the initial kinetic energy is at a low wave number.

because the only freedom that we had to work with was the form of the interpolated "cell-wall" value, which will be denoted here by $\hat{A}$. Once we chose $\hat{A}$ so as to conserve, say, A^2 , we had no room left to maneuver, so we could not conserve anything else.

We have just shown, however, that the vorticity equation for two-dimensional nondivergent flow can be discretized so as to conserve two quantities, namely the kinetic energy and the enstrophy, in addition to the vorticity itself. How is that possible?

The key difference with the vorticity equation is that we can choose not only how to interpolate the vorticity (so as to conserve the enstrophy), but also *the actual finite-difference expression for the advecting wind itself*, in terms of the stream function, because that expression is implicit in the form of the Jacobian that we use. In choosing the form of the advecting current, we have a second "freedom," which allows us to conserve a second quantity, namely the kinetic energy.

As discussed earlier, the constraint of enstrophy conservation is needed to ensure that kinetic energy does not cascade in two-dimensional nondivergent flow. If kinetic energy does not cascade, the flow remains smooth. When the flow is smooth, kinetic energy conservation is approximately satisfied, even if it is not exactly guaranteed by the scheme. This means that a scheme that exactly conserves enstrophy and approximately conserves kinetic energy will behave well.

These considerations suggest that formal enstrophy conservation is "more important" than formal kinetic energy conservation.

11.6 Angular momentum conservation

Finally, for completeness, define the relative angular momentum per unit mass, M, by

$$M_{rel} \equiv ua\cos\varphi \,. \tag{124}$$

This is actually the component of the relative angular momentum vector in the direction of the axis of the Earth's rotation. Here we consider motion on the sphere, a is the radius of the Earth, and u is the zonal component of the wind. From the momentum equation we can show that in the absence of pressure-gradient forces and friction,

$$\frac{\partial M}{\partial t} = -\left(\mathbf{V}\cdot\nabla\right)M \,, \tag{125}$$

where λ is longitude, and

$$M \equiv M_{rel} + \Omega a^2\cos\varphi \tag{126}$$

is the component of the absolute angular momentum vector in the direction of the axis of the Earth's rotation. From (125) it follows that the absolute angular momentum is conserved under advection.

Using integration by parts, it can be demonstrated that

$$\overline{M_{rel}} = a^2\int_{-\frac{\pi}{2}}^{\frac{\pi}{2}}\int_0^{2\pi}\varsigma\sin\varphi\cos\varphi d\lambda d\varphi \,. \tag{127}$$

We can also prove that

$$\frac{d}{dt}\overline{M_{rel}} = a^2\int_{-\frac{\pi}{2}}^{\frac{\pi}{2}}\int_0^{2\pi}\frac{\partial\varsigma}{\partial t}\sin\varphi\cos\varphi d\lambda d\varphi = 0 \,. \tag{128}$$

This means that angular momentum is conserved.

11.7 Conservative schemes for the two-dimensional shallow water equations with rotation

The approach outlined below follows Arakawa and Lamb (1981). We adopt the C-grid, as shown in Fig. 11.12. Recall that on the C-grid, the zonal winds are east and west of the mass points, and the meridional winds are north and south of the mass points. The divergence "wants" to be defined at mass points, e.g., at point $(i + 1/2, j + 1/2)$; and the vorticity "wants" to be defined at the corners of the mass boxes that lie along the diagonal lines connecting mass points, e.g., at the point (i, j).

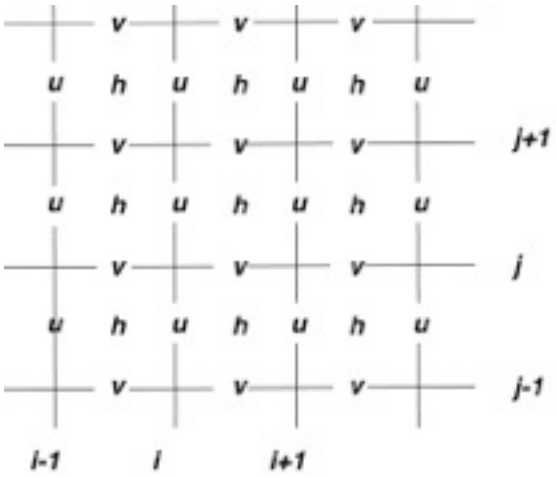

Figure 11.12: The arrangement of the mass, zonal wind, and meridional wind on the C grid.

The finite-difference form of the continuity equation is

$$\frac{dh_{i+\frac{1}{2},j+\frac{1}{2}}}{dt} = \frac{(hu)_{i,j+\frac{1}{2}} - (hu)_{i+1,j+\frac{1}{2}}}{\Delta x} + \frac{(hv)_{i+\frac{1}{2},j} - (hv)_{i+\frac{1}{2},j+1}}{\Delta y} . \tag{129}$$

The various mass fluxes that appear in (129) have not yet been defined, but mass will be conserved regardless of how we define them.

Simple finite-difference analogs of the two components of the momentum equation are

$$\frac{du_{i,j+\frac{1}{2}}}{dt} - \left[\left(\frac{\zeta + f}{h}\right)(hv)\right]_{i,j+\frac{1}{2}} + \left(\frac{K_{i+\frac{1}{2},j+\frac{1}{2}} - K_{i-\frac{1}{2},j+\frac{1}{2}}}{\Delta x}\right) + g\left[\frac{(h+h_s)_{i+\frac{1}{2},j+\frac{1}{2}} - (h+h_s)_{i-\frac{1}{2},j+\frac{1}{2}}}{\Delta x}\right] = 0 , \tag{130}$$

and

$$\frac{dv_{i+\frac{1}{2},j}}{dt}+\left[\left(\frac{\zeta+f}{h}\right)(hu)\right]_{i+\frac{1}{2},j}+\left(\frac{K_{i+\frac{1}{2},j+\frac{1}{2}}-K_{i+\frac{1}{2},j-\frac{1}{2}}}{\Delta y}\right)+g\left[\frac{(h+h_S)_{i+\frac{1}{2},j+\frac{1}{2}}-(h+h_S)_{i+\frac{1}{2},j-\frac{1}{2}}}{\Delta y}\right]=0\,,$$

(131)

respectively. As in the one-dimensional case, the kinetic energy per unit mass, $K_{i+\frac{1}{2},j+\frac{1}{2}}$, is undefined at this stage, but resides at mass points. The potential vorticities $\left(\frac{\zeta+f}{h}\right)_{i,j+\frac{1}{2}}$ and $\left(\frac{\zeta+f}{h}\right)_{i+\frac{1}{2},j}$, and the mass fluxes $(hv)_{i,j+\frac{1}{2}}$ and $(hu)_{i+\frac{1}{2},j}$ are also undefined.

Note that on the C-grid the mass fluxes that appear in (130) and (131) are in the "wrong" places; the mass flux $(hv)_{i,j+\frac{1}{2}}$ that appears in the equation for the *u*-wind is evidently at a *u*-wind point, and the mass flux $(hu)_{i+\frac{1}{2},j}$ that appears in the equation for the *v*-wind is evidently at a *v*-wind point. The vorticities that appear in (130) and (131) are also in the "wrong" places. Obviously, what we have to do is interpolate somehow to obtain mass fluxes and vorticities suitable for use in the vorticity terms of (130) and (131). Note, however, that it is actually *products* of mass fluxes and vorticities that are needed.

One obvious and important question is: *Is there a finite-difference scheme that allows us to "mimic" the identity (8), i.e.,* $(h\mathbf{V})\cdot\left[\mathbf{k}\times(h\mathbf{V})\right]=0$ *?* Since (8) is a purely mathematical identity, the input variables are irrelevant, and the approach is to mimic the identity itself. Arakawa and Lamb constructed the finite-difference vorticity terms in such a way that a finite-difference analog to (8) is satisfied, regardless of the specific forms of the mass fluxes and potential vorticities that are chosen. They constructed the vorticity terms as follows:

$$\begin{aligned}\left[\left(\frac{\zeta+f}{h}\right)(hv)\right]_{i,j+\frac{1}{2}} &= \alpha_{i,j+\frac{1}{2};i+\frac{1}{2},j+1}(hv)_{i+\frac{1}{2},j+1}+\beta_{i,j+\frac{1}{2};i-\frac{1}{2},j+1}(hv)_{i-\frac{1}{2},j+1}\\ &+\gamma_{i,j+\frac{1}{2};i-\frac{1}{2},j}(hv)_{i-\frac{1}{2},j}+\delta_{i,j+\frac{1}{2};i+\frac{1}{2},j}(hv)_{i+\frac{1}{2},j}\end{aligned}$$

(132)

and

$$\begin{aligned}\left[\left(\frac{\zeta+f}{h}\right)(hu)\right]_{i+\frac{1}{2},j} &= \gamma_{i+\frac{1}{2},j;i+1,j+\frac{1}{2}}(hu)_{i+1,j+\frac{1}{2}}+\delta_{i+\frac{1}{2},j;i,j+\frac{1}{2}}(hu)_{i,j+\frac{1}{2}}\\ &+\alpha_{i+\frac{1}{2},j;i,j-\frac{1}{2}}(hu)_{i,j-\frac{1}{2}}+\beta_{i+\frac{1}{2},j;i+1,j-\frac{1}{2}}(hu)_{i+1,j-\frac{1}{2}}\,.\end{aligned}$$

(133)

In reality, the forms assumed by Arakawa and Lamb are slightly more general and slightly more complicated than these; we simplify here for ease of exposition. In (132) and (133), the α 's, β 's, γ 's, and δ 's obviously represent interpolated potential vorticities whose forms are not yet specified. Each of these quantities has four subscripts, to indicate that it links a specific *u*-wind point with a specific *v*-wind point. The α 's, β 's, γ 's, and δ 's are somewhat analogous to the *a*'s and *b*'s that were defined in the discussion of two-dimensional non-divergent flow, in that the *a*'s and *b*'s also linked pairs of points. In (132), the interpolated potential vorticities multiply the mass fluxes hv at the four *v*-wind points surrounding the *u*-wind point $\left(i, j+\frac{1}{2} \right)$, and similarly in (133), the interpolated potential vorticities multiply the mass fluxes hu at the four *u*-wind points surrounding the *v*-wind point $\left(i+\frac{1}{2}, j \right)$.

When we form the kinetic energy equation, we have to take the dot product of the vector momentum equation with the mass flux $h\mathbf{V}$. This means that we have to multiply (132) by $(hu)_{i+\frac{1}{2},j}$ and (133) by $(hv)_{i,j+\frac{1}{2}}$, and add the results. With the forms given by (132) and (133), the vorticity terms will sum to

$$
\begin{aligned}
&-(hu)_{i,j+\frac{1}{2}}\left[\left(\frac{\zeta+f}{h}\right)(hv)\right]_{i,j+\frac{1}{2}}+(hv)_{i+\frac{1}{2},j}\left[\left(\frac{\zeta+f}{h}\right)(hu)\right]_{i+\frac{1}{2},j} \\
&=-(hu)_{i,j+\frac{1}{2}}\left[\alpha_{i,j+\frac{1}{2};i+\frac{1}{2},j+1}(hv)_{i+\frac{1}{2},j+1}+\beta_{i,j+\frac{1}{2};i-\frac{1}{2},j+1}(hv)_{i-\frac{1}{2},j+1}+\gamma_{i,j+\frac{1}{2};i-\frac{1}{2},j}(hv)_{i-\frac{1}{2},j}+\delta_{i,j+\frac{1}{2};i+\frac{1}{2},j}(hv)_{i+\frac{1}{2},j}\right] \\
&+(hv)_{i+\frac{1}{2}\cdot j}\left[\gamma_{i+\frac{1}{2},j;i+1,j+\frac{1}{2}}(hu)_{i+1,j+\frac{1}{2}}+\delta_{i+\frac{1}{2},j;i,j+\frac{1}{2}}(hu)_{i,j+\frac{1}{2}}+\alpha_{i+\frac{1}{2},j;i,j-\frac{1}{2}}(hu)_{i,j-\frac{1}{2}}+\beta_{i+\frac{1}{2},j;i+1,j-\frac{1}{2}}(hu)_{i+1,j-\frac{1}{2}}\right].
\end{aligned}
\tag{134}
$$

Inspection of (134) makes it clear that cancellation will occur when we sum over the grid. This means that the vorticity terms will drop out of the finite-difference kinetic energy equation, just as they drop out of the continuous kinetic energy equation. This cancellation will occur regardless of the expressions that we choose of the mass fluxes, and regardless of the expressions that we choose for the α 's, β 's, γ 's, and δ 's. The cancellation arises purely from the forms of (132) and (133), and is analogous to the cancellation that makes (8) work, i.e.,

$$
A\mathbf{V}\cdot(\mathbf{k}\times\mathbf{V})=A(u\mathbf{i}+v\mathbf{j})\cdot(-v\mathbf{i}+u\mathbf{j})=A(-uv+uv)=0\,,
\tag{135}
$$

regardless of the input quantities *A* and **V**. This is yet another example of "mimetic discretization."

The above discussion shows that the finite-difference momentum equations represented by (130) and (131) with the use of (132) and (133), will guarantee kinetic energy conservation under advection, regardless of the forms chosen for the mass fluxes and the interpolated potential vorticities α , β , γ , and δ . From this point, the methods used in the discussion of the one-dimensional purely divergent flow will carry through essentially without change to give us conservation of mass, potential energy, and total energy. Arakawa and Lamb (1981) went much further, however, showing how the finite-difference momentum equations presented above (or, actually, slightly generalized versions of these equations) allow conservation of both potential vorticity and potential enstrophy. The details are rather complicated and will not be presented here.

11.8 The effects of time differencing on energy conservation

A family of finite-difference schemes for (27) can be written in the generic form

$$\frac{q_{i,j}^{\,n+1} - q^{n}_{\,i,j}}{\Delta t} = J_{i,j}\left(q^{*},\psi\right), \tag{136}$$

where $J_{i,j}$ is a finite difference analog to the Jacobian at the point (i,j), and different choices of q^{*} give different time-differencing schemes. Examples are given in Table 11.1. Multiplying (136) by q^{*}, we get

$$q^{*}\left(q^{n+1} - q^{n}\right) = \Delta t q^{*} J\left(q^{*},\psi\right), \tag{137}$$

or, after some algebraic sleight-of-hand,

$$\left(q^{n+1}\right)^{2} - \left(q^{n}\right)^{2} = 2\left(\frac{q^{n+1} + q^{n}}{2} - q^{*}\right)\left(q^{n+1} - q^{n}\right) + 2\Delta t q^{*} J\left(q^{*},\psi\right). \tag{138}$$

The left-hand side of (138) represents the change of q^2 in one time step. Consider the summation of q^2 over all grid points, divided by the number of grid points, and let this mean be denoted by an overbar. We find that

$$\overline{\left(q^{n+1}\right)^{2}} - \overline{\left(q^{n}\right)^{2}} = \overline{2\left(\frac{q^{n+1} + q^{n}}{2} - q^{*}\right)\left(q^{n+1} - q^{n}\right)} + 2\Delta t\,\overline{q^{*} J\left(q^{*},\psi\right)}, \tag{139}$$

which shows that the change of the mean-square of q depends on two terms. The first involves the choice of q^{*}, so this is where the time-differencing comes in. For $q^{*} = q^{n}$, the contribution of

this term is positive and so tends to increase $\overline{q^2}$. On the other hand, for $q^* = q^{n+1}$, the contribution is negative and so tends to decrease $\overline{q^2}$. If we use the trapezoidal scheme, which is absolutely stable and neutral (in the linear case with constant coefficients), there is no contribution from the first term. This means that the trapezoidal scheme is consistent with (allows) exact energy conservation. This could be anticipated given the time-reversibility of the trapezoidal scheme, which was discussed earlier. Of course, the form of the finite-difference Jacobian must also be consistent with energy conservation.

Name of Scheme	Form of Scheme
Euler forward	$q^* = q^n$
Backward implicit	$q^* = q^{n+1}$
Trapezoidal implicit	$q^* = \frac{1}{2}\left(q^n + q^{n+1}\right)$
Leapfrog, with time interval $\Delta t / 2$	$q^* = q^{n+\frac{1}{2}}$
Second-order Adams Bashforth	$q^* = \frac{3}{2}q^n - \frac{1}{2}q^{n-1}$
Heun	$q^* = q^n + \frac{\Delta t}{2} J\left(q^n, \psi\right)$
Lax-Wendorff (here *S* is a smoothing operator)	$q^* = Sq^n + \frac{\Delta t}{2} J\left(q^n, \psi\right)$
Matsuno	$q^* = q^n + \Delta t J\left(q^n, \psi\right)$

Table 11.1: Examples of time differencing schemes obtained through various choices of q^*.

In most cases, time truncation errors that interfere with exact energy conservation do not cause serious problems, provided that the scheme is stable in the linear sense, e.g., as indicated by von Neumann's method.

11.9 Summary

We began this chapter by discussing two-dimensional advection. When the advecting current is variable, a new type of instability can occur, which can be called "aliasing instability."

In practice, it is often called "non-linear instability." This type of instability occurs regardless of the time step, and cannot be detected by von Neumann's method. It can be detected by the energy method, and it can be controlled by enforcing conservation of appropriate quadratic variables, such as energy or enstrophy. It is particularly likely to cause trouble with the momentum equations, which describe how the wind is "advected by itself." Conservation of potential vorticity is an extremely important dynamical principle, as discussed in courses on atmospheric dynamics. Conservation of potential enstrophy is key to determining the distribution of kinetic energy with scale. Schemes that permit conservation of potential vorticity and potential enstrophy under advection therefore provide major benefits in the simulation of geophysical circulations.

Problems

1. A wagon wheel rotates at R revolutions per second. It is featureless except for a single dot painted near its outer edge. The wheel is filmed at F frames per second.

a) What inequality must F satisfy to avoid aliasing?

b) How does the *apparent* rotation rate, R^*, vary as a function of F and R? Assume $R > 0$ and $F > 0$.

2. Prove that J_1 satisfies (90). Assume periodic boundary conditions.

3. Prove that J_3 gives kinetic energy conservation for the case of two-dimensional nondivergent flow. Assume periodic boundary conditions.

4. Prove that J_2 gives exact vorticity conservation (ignoring time truncation error). Assume periodic boundary conditions.

5. Work out the *continuous* form of the Jacobian for the case of spherical coordinates (longitude, λ, and latitude, φ).

6. For the case of two-dimensional non-divergent flow on a periodic domain, prove that if the vorticity is an eigensolution of the Laplacian, then the time-rate-of-change of the vorticity is zero.

7. Using the form of the Laplacian for the hexagonal grid that you worked out earlier in the semester, and using a suitable definition of the kinetic energy at the cell centers (which you must invent), show that Eq. (108) of the notes can be satisfied. Note that (108) need only hold *for the sum over all grid points*, as shown.

8. For a hexagonal grid, show that a finite-difference Jacobian of the form

$$\frac{d\zeta_0}{dt} = \frac{1}{A}\sum_{i=1}^{6}\left(\frac{\psi_{i+1}-\psi_{i-1}}{\Delta s}\right)\left(\frac{\varsigma_0+\varsigma_i}{2}\right)\Delta s \tag{140}$$

conserves vorticity, enstrophy, and kinetic energy when used with the nondivergent barotropic vorticity equation. Here subscript 0 denotes the central point, the sum is over the six surrounding points (assumed to be numbered consecutively in a counter-clockwise fashion), A is the area of a hexagon, and Δs is the length of a side.

9.

a) Make a finite-difference model that solves the non-divergent vorticity equation on a doubly periodic plane, using an approximately square hexagonal grid with about 8000 grid cells, like the one used in the Chapter 2 homework. Use the Jacobian given by (140), with Matsuno time differencing. You should check your Jacobian code by using a test function for which you can compute the Jacobian analytically.

b) Create diagnostics for the domain-averaged enstrophy and kinetic energy.

c) Invent an analytical function that you can use to specify an initial condition such that the periodic domain contains two pairs of (nearly) circular large-scale vorticies of equal strength but opposite sign -- two "highs" and two "lows." Because of the periodic boundary conditions, the solution will actually represent infinitely many vortices. Run the model with this smooth initial condition and discuss the results.

d) Run the model again using initial conditions that approximate "white noise," and examine the time evolution of the solution. Does it follow the behavior expected for two-dimensional turbulence? You may have to run a thousand time steps or more to see the expected evolution.